Journal of Engineering Science and Technology Review 17 (4) (2024) 50-57

Research Article

JOURNAL OF
Engineering Science and Technology Review

www.jestr.org

A New Combined Splicing Joint for Shield Segment

Jiaqi Sun[1], Xu Chang[1,*] and Mintae Kim[2]

[1]*School of Civil Engineering, Huaqiao University, Xiamen 361021, China*
[2]*School of Civil, Environmental, and Architectural Engineering, Korea University, Seoul 02841, Republic of Korea*

Received 11 May 2024; Accepted 19 August 2024

Abstract

Tunnel accidents caused by water leakage are closely related to the segmental joints, and it is therefore significant to control joint deformation. The traditional segmental joints cannot provide sufficient stiffness and strength in complex geological conditions. To solve these problems, in this study, a type of plug-in joint (composed of a sleeve and a pin) was added to the traditional segmental joints and worked in conjunction with the bolts to form a new type of combined splicing joint. The combined splicing joint was tested under four-point bending conditions. Results show that the combined splicing joint can improve the bending stiffness and load capacity of the structure. The number and position of the plug-in joints clearly affect the load capacity of the segmental joint. This study then develops an analytical method to predict the load capacity and bending stiffness of the combined splicing joints. The new combined splicing joint can effectively reduce the deformation of the segmental joints.

Keywords: Shield tunnel, Deformations, Combined splicing joint, Ultimate load capacity

1. Introduction

The shield tunneling machine has been extensively adopted in tunnel construction due to its convenient construction procedure, enhanced safety technologies, and reduced labor intensities. In many cases, the segments of the shield tunnel undergo different transversal movements in the longitudinal direction during the construction process. Research has also found that pore water pressure, spatial variability of soil properties, and segment uplift are common causes [1-2]. As a result, concrete cracking and leakages can often be found near the segmental joints, leading to a series of problems such as the decrease in the overall stiffness and plastic bearing range of the lining structures, threatening the security of the shield tunnel [3]. Therefore, the segmental joints have been regarded as the weakest part of the segmental structure in terms of serviceability, because their stiffness and strength are lower than those of the main segments, and they are more prone to water and gas leakage. Their mechanical performances will determine the overall behavior of the lining structures. Consequently, the exploration of the mechanical performances of these segmental joints has become a research hotspot.

Steel fiber has been widely applied in shield tunnel engineering due to its advantages of high strength and labor reduction. Adding steel or other fibers into the concrete to form fiber-reinforced concrete can significantly improve the tensile strength and crack resistance of segments, and further enhance the overall durability of the lining structures [4]. In the context of tunnel engineering, particularly those involving shield tunneling techniques, the structural integrity and long-term safety of the lining structure are paramount. The lining, consisting of precast concrete segments, serves as the primary barrier between the tunnel's interior and the surrounding ground, providing stability and protection against water ingress, soil movements, and other environmental factors. Traditionally, steel fibers and polymer fibers have been incorporated into the concrete mix to enhance the mechanical properties of the segments themselves, such as improving their tensile strength, flexural strength, and durability. However, while these fiber-reinforced concretes have proven effective in strengthening the individual segments, they have had limited impact on improving the load-bearing capacity and overall performance of the segmental joints, which are the weak links in the lining system.

Segmental joints, where the individual concrete segments are bolted or otherwise fastened together, are crucial for the structural continuity and overall stability of the tunnel lining. However, these joints are inherently weaker than the segments themselves and are more prone to damage and failure under load or due to environmental factors. As such, the load capacity of the entire lining structure is often governed by the strength and performance of the segmental joints. Given these limitations, there is a pressing need to develop innovative solutions that can enhance the strength and durability of the segmental joints. One such approach is the use of external reinforcement methods, such as bonding steel or fiber-reinforced polymer reinforcement to the joints. While these methods can provide some degree of strengthening in cases where significant deformations have already occurred, they are often seen as remedial measures rather than fundamental solutions [5, 6].

A more sustainable and effective approach would be to design and develop a new type of segmental joint that inherently possesses higher strength and resilience. Such a joint would not only be capable of withstanding higher loads but would also be better equipped to resist environmental degradation and maintain its integrity over the life of the tunnel. The development of such a joint would involve a multidisciplinary approach, drawing on expertise in materials science, engineering mechanics, and tunnel

*E-mail address: changxu815@163.com
ISSN: 1791-2377 © 2024 School of Science, DUTH. All rights reserved.
doi:10.25103/jestr.174.07

construction techniques. Potential areas of investigation could include the use of advanced materials and composites for the joint interfaces, the design of innovative fastening mechanisms, and the implementation of monitoring and maintenance strategies to ensure the long-term performance of the joints [7, 8].

The development of a new type of segmental joint with enhanced strength and durability has the potential to significantly improve the design and structural safety of lining structures in shield tunnels. By addressing the weak link in the system, such a joint could help to reduce the risk of accidents and extend the service life of tunnel infrastructure, ultimately benefiting the public and reducing the costs associated with maintenance and repairs.

2. State of the art

Significant efforts have been devoted to investigating tunnel segmental joints through laboratory tests, numerical simulations, and analyses. Liu et al. [9] tested the mechanical performances of continuously jointed segments and discovered that the lining structures typically failed due to compression crushing of the joint concrete. They emphasized that optimizing the structural design of tunnel linings necessitates improving the strength of segmental joints. Gong et al. [4] conducted a comprehensive study comparing traditional segmental joints with fiber-reinforced concrete segmental joints and found that the latter exhibited higher load capacity, initial cracking load, and narrower crack widths. Rashiddel et al. [10] analyzed segmental tunnel linings using two numerical methods: the beam-spring method and the solid-interface method. Zhang et al. [11] analyzed the parameters affecting the bending capacity of segmental joints and found that the width of the segment, as well as the size and number of bolts, significantly influenced their bending ability. Avanaki et al. [12] separately investigated the flexural behavior of segmental joints and their performance under tunnel-boring machine thrust forces for Hybrid steel fiber-reinforced concrete (HSFRC) segments through experimental and numerical approaches.

Other scholars Guo et al. [13] conducted tests on segmental joints under bending conditions, and numerous numerical simulations were also performed based on sophisticated numerical models to further capture the failure process of the joints. Zhang et al. [14] numerically investigated segmental joints and validated their model with full-scale tests. Their research results indicated that bolt stress was controlled by joint opening and vertical displacement, while the preload of the bolt had no apparent effect on the change in segmental joint deformation with bending moment. Oh and Moon [15] conducted a seismic analysis of longitudinal tunnel and ground response using three-dimensional quasi-static linear elastic and nonlinear elastic discrete beam-spring elements to represent the segmental liner and ground spring, respectively. Boye et al. [16] assessed the accuracy of published equations for bursting force and peak stress through high-resolution two-dimensional finite element-based parametric studies. Allahverdi et al. [17] presented the results of three-dimensional advanced finite element modeling for one of the major ongoing construction projects in the North America. They discussed the critical responses such as ground deformation, settlement trough, crown deformation, and the internal forces in the linings considering different segment joint modeling. Yang et al. [18] investigated the mechanical performances of segments of steel fiber reinforced concrete based on a three-dimensional mesoscale numerical model with randomly distributed steel fibers. Analytical methods were also frequently employed to investigate the mechanical performances of segmental joints, with the equivalent continuous model and the beam-spring model being two commonly adopted approaches.

In addition to the aforementioned tests and numerical simulations focusing on the mechanical properties of segmental joints, numerous studies have been conducted from other perspectives. An automatic structural health monitoring system has been developed to monitor the opening of segmental joints, mitigate the risk of damage, and ensure the safety of shield tunnels. Currently, there is extensive research on strengthening reinforced concrete structures by adhering FRP materials to their surfaces [19, 21]. This method is also applicable to strengthening segmental joints. However, strengthening the bolts, which are crucial components of segmental joints, represents a more direct approach. Nevertheless, the aforementioned method can still provide valuable guidance [22, 26].

These studies have enhanced our understanding of the mechanical performances of segmental joints, leading to improved design quality and increased safety. Notably, these methods do not significantly contribute to the load capacity of segmental joints, which primarily depends on the bolts connecting the segments [27, 30]. Therefore, a novel plug-in joint has been introduced at the interface between segments. This joint works in conjunction with the bolts to form a new type of combined splicing joint..

This study is arranged as follows. In Section 3, the test arrangements for the combined splicing joint are introduced. In Section 4, the test results of suggested joints are analyzed and described, and theoretical calculation formulas for the new combined splicing joints are also given. And then the conclusions are summarize in Section 5.

3. Methodology

3.1 Test specimens

The proposed combined splicing joint comprises two distinct types of joints: one for the traditional bolt joint and the other for the plug-in joint. The pin part and the sleeve part are embedded in two separate segments, respectively (Fig. 1). During the construction process, the two segments can be effortlessly connected using the plug-in joint, thereby enhancing the joint's capacity.

In this study, a total of four test specimens were tested. All four specimens have identical dimensions: an outer radius of 1500 mm and an inner radius of 1350 mm, a width of 600 mm, and a center angle of 67.5°. The steel used is of Q235B grade, and the concrete for the four segments is uniform, with a strength grade of C50. Each segment is equipped with two hand holes and two bolt holes for installing bolts. In addition to these holes, different numbers of plug-in joints are also incorporated.

Specifically, two ordinary segments are spliced together using two bolts to form an ordinary segmental joint, labeled as JT0. For JT1, one plug-in joint is embedded; for JT2, two; and for JT3, three. The bolts are 240 mm long straight bolts, and the plug-in joints are made of No. 45 steel. Figs. 1(d) and 1(e) illustrate the cross-sectional and circumferential structures of the combined splicing joint sleeve end, respectively.

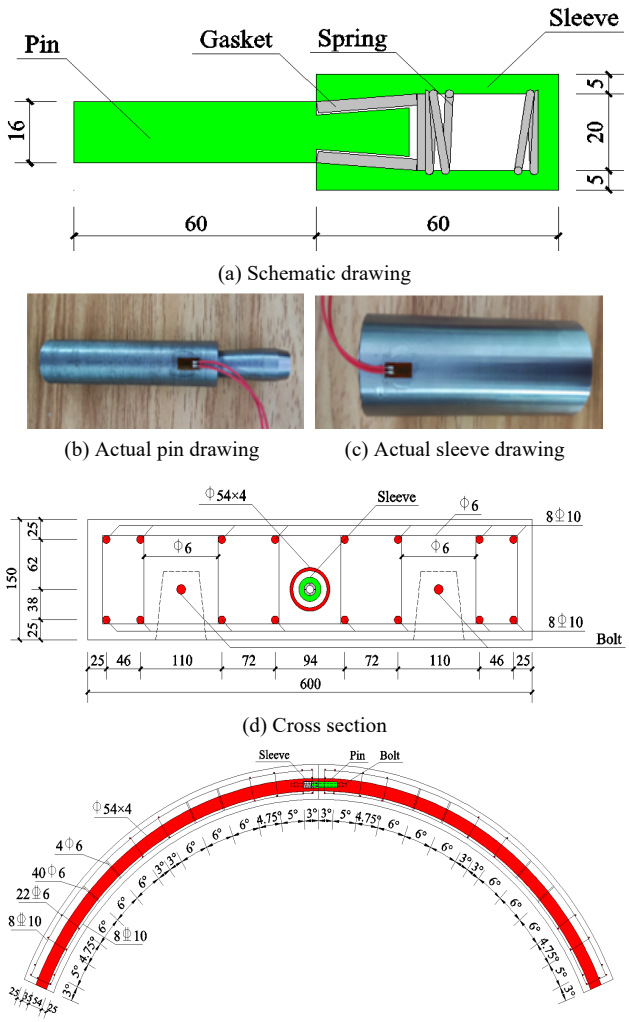

(a) Schematic drawing

(b) Actual pin drawing

(c) Actual sleeve drawing

(d) Cross section

(e) Circumferential section

Fig. 1. Plug-in joint structure

3.2 Test methods

The segmental joints are tested using a large self-reaction test frame. All specimens undergo testing under four-point bending conditions. The arrangement of the jack, distribution beam, pressure rods, and rubber pads during the test process is shown in Fig. 2. Vertical displacement sensors are positioned on both sides of the segmental joint's inner arc surface to measure its vertical deformation. Horizontal displacement sensors are arranged on both the inner and outer arc surfaces of the segmental joints to measure their opening displacement. Fig. 2 presents a sketch of the segmental joint bending performance test device.

The loading method for the segments is identical to that described in the previous section. During the loading process, the displacement of each measurement point is recorded after the load holding time has elapsed. Additionally, the development of cracks on the inner and outer arc surfaces of the segmental joints is observed and recorded.

4. Results analysis and discussion

4.1 Test results

The plug-in joints for JT1, JT2, and JT3 are installed at the centroid positions of the segment components. The load-deflection curves obtained from the test results of the four types of segmental joint models are presented in Fig. 3. It can be observed that incorporating a plug-in joint into the segmental joint enhances its capacity, and as the number of plug-in joints increases, the improvement in capacity becomes more pronounced.

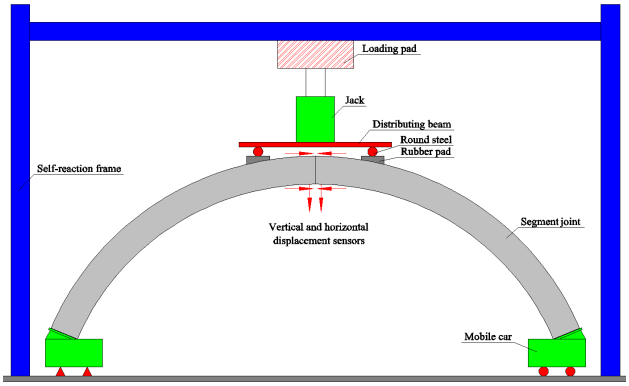

(a) Schematic drawing

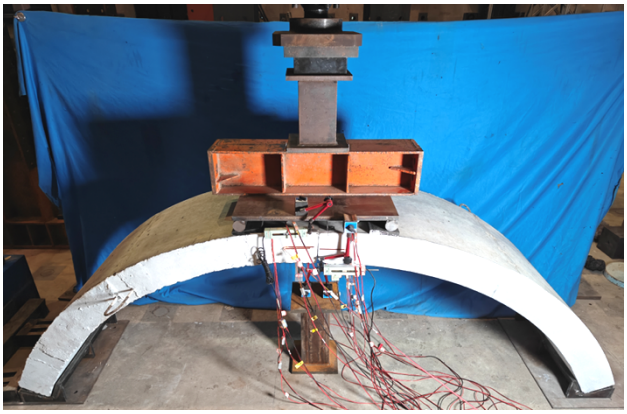

(b) Test arrangement

Fig. 2. Sketch of the segmental joint bending performance test device

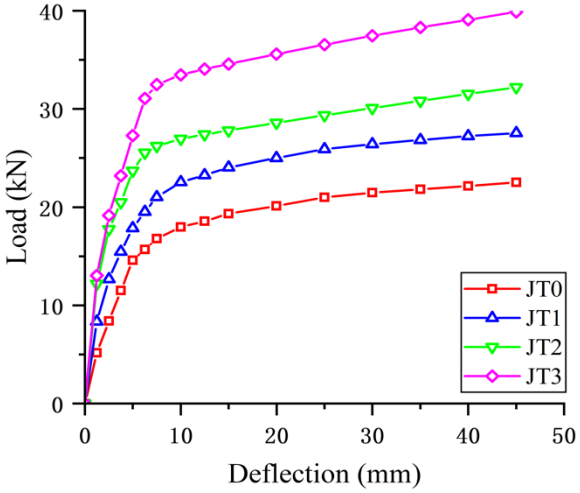

Fig. 3. Load-deflection curves of the segmental joints with different numbers of plug-ins

To further analyze the influence of the number of plug-ins on the joint's capacity, the results of the load capacity for the four types of joints are listed in Table 1. Additionally, the increase in load capacity between different segmental joints is calculated. As shown in Table 1, after adding 3 plug-in joints, the load capacity increases by 71.4% compared to the segmental joint without any plug-in joints.

Table 1. Load capacity of the segmental joints with different numbers of plug-in joints

Number of plug-in joint	Ultimate load (kN)	Increase (%)
0	21	–
1	26	23.8
2	30	42.9
3	36	71.4

To analyze the influence of different plug-in joint positions on the joint's capacity, specimens JT4, JT5, and JT6 were designed. The distances between the centroid of the plug-in joints and the inner arc surface of the segment are 53 mm, 63 mm, and 73 mm, respectively. Since the position of the plug-in joints in the combined splicing joint designed in this paper aligns with that of the bolts, the position of the bolts changes accordingly with the position of the plug-in joints. As the plug-in joints are installed at the centroid of the concrete, and all other parameters remain unchanged, the load-deflection relationships of the segmental joints are presented in Fig. 4.

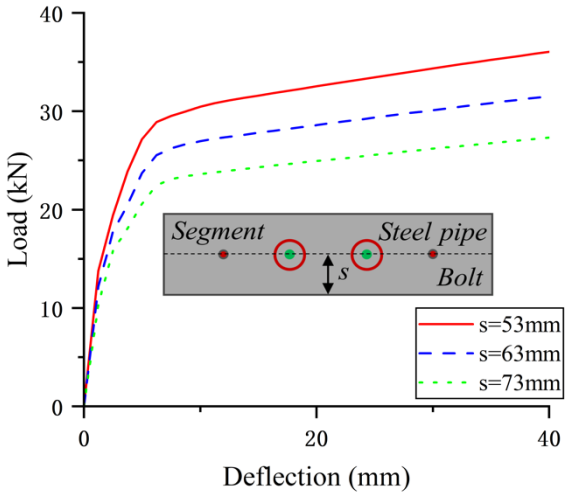

Fig. 4. Load-deflection curves of the segmental joints with different positions of the plug-in joints

Fig. 4 reveals that adjusting the position of the plug-in joints significantly impacts the load capacity of the segmental joint. Specifically, a closer proximity of the plug-in joints to the inner arc surface of the segment results in a higher load capacity, whereas a greater distance leads to a decrease in load capacity. This suggests that optimizing the position of the plug-in joints can effectively enhance the load capacity of the segmental joint.

4.2 Theoretical calculation

4.2.1 Basic assumptions

The segment joint is simplified into a beam model, where the bolts are treated as steel bars. The load capacity of the normal section is calculated based on the following fundamental assumptions: The plane section remains plane (plane section assumption. The tensile strength of the concrete is neglected. The stress-strain relationship of the concrete under compression is determined by Eq. (1).

These assumptions form the basis for calculating the load capacity of the segment joint, which is crucial for understanding its structural behavior and ensuring its safety and performance.

$$\sigma_c = \begin{cases} f_c\left[1-\left(1-\dfrac{\varepsilon_c}{\varepsilon_0}\right)^n\right], & \varepsilon_c \le \varepsilon_0 \\ f_c, & \varepsilon_0 < \varepsilon_c \le \varepsilon_{cu} \end{cases} \tag{1}$$

where σ_c and ε_c are the stress and strain for the concrete under compressive conditions and f_c is the designed compressive strength. ε_0 is the concrete compressive strain, which is calculated according to Eq. (2). Its minimum value is 0.02.

$$\varepsilon_0 = 0.002 + 0.5\left(f_{cu,k} - 50\right)\times 10^{-5} \tag{2}$$

where ε_{cu} is the ultimate compressive strain of the normal section, which is calculated by Eq. (3). When the concrete is under nonuniform compression and the value calculated by Eq. (3).

$$\varepsilon_{cu} = 0.0033 - \left(f_{cu,k} - 50\right)\times 10^{-5} \tag{3}$$

where n is the coefficient, which is calculated according to Eq. (4). And its maximum value is 2.0.

$$n = 2 - \frac{1}{60}\left(f_{cu,k} - 50\right) \tag{4}$$

where $f_{cu,k}$ is the standard compressive strength value of the concrete cube.

It can be calculated that $\varepsilon_0 = 0.002$, $\varepsilon_{cu} = 0.0033$, and $n = 2$.

To simplify the formula derivation, the compressive stress-strain response before the peak strength of the concrete is simplified into a linear model:

$$\sigma_c = \begin{cases} E_{ce}\varepsilon_c, & \varepsilon_c \le \varepsilon_0 \\ f_c, & \varepsilon_0 < \varepsilon_c \le \varepsilon_{cu} \end{cases} \tag{5}$$

where E_{ce} is the secant modulus (deformation modulus) of the concrete, which is determined by Eq. (6). $E_{ce} = 11.6\text{GPa}$ when the concrete grade is C50.

$$E_{ce} = \frac{f_c}{\varepsilon_0} \tag{6}$$

By simplifying the bolt and plug-in joint into elastic–ideal plastic materials, the tensile stress–strain response of the bolt is expressed as follows:

$$\sigma_{st}=\begin{cases}E_s\varepsilon_{st}, \varepsilon_{st}\tilde{N}\varepsilon_y\\ f_y, \varepsilon_y<\varepsilon_{st}\tilde{N}\varepsilon_u\end{cases} \tag{7}$$

The tension stress and strain relationship of the plug-in joint is taken as follows:

$$\sigma_{sj}=\begin{cases}E_{sj}\varepsilon_{sj}, \varepsilon_{sj}\tilde{N}\varepsilon_{yj}\\ f_{yj}, \varepsilon_{yj}<\varepsilon_{sj}\tilde{N}\varepsilon_{uj}\end{cases} \tag{8}$$

where σ_{st} and ε_{st} are the bolt tensile stress and strain, respectively; σ_{sj} is the tension stress of the plug-in joint when the strain of the plug-in joint is ε_{sj}; E_s and E_{sj} are the elastic moduli of the bolt and the plug-in joint, respectively; f_y and f_{yj} are the tension yield strength design values of the bolt and the plug-in joint, respectively; ε_y and ε_{yj} are the tension yield strains of the bolt and the plug-in joint, respectively; and ε_u and ε_{uj} are the ultimate tension strains of the bolt and the plug-in joint, respectively.

When shield tunnel segments are in service in the stratum, the stress distribution at the joint is shown in Fig. 5.

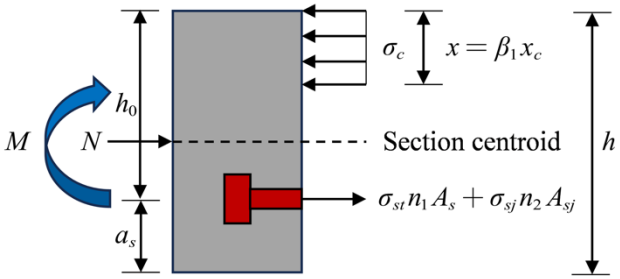

Fig. 5. Diagram of the force at the joint of the combined splicing joint

Through the equilibrium relationship of the horizontal force, it can be concluded that:

$$N+\sigma_{st}n_1A_s+\sigma_{sj}n_2A_{sj}=\sigma_c bx \tag{9}$$

where N is the axial force of segments; b represents the segment width; σ_c is the concrete compressive stress obtained via the equivalent rectangular stress pattern; x represents the height of the compressive zone; n_1 and n_2 represent the number of bolts and plug-in joints, respectively; and A_s and A_{sj} represent the effective sectional areas of the bolt and plug-in joints, respectively.

For the reinforced concrete structure, the stress and strain in the compressive zone should reach the compressive strength and the ultimate strain, respectively. Additionally, the bolt tensile stress should reach the bolt's yield strength, and the plug-in joint should reach its yield strength. The stress and strain of the concrete are related as follows:

$$\begin{cases}\sigma_c\tilde{N}\alpha_1 f_c\\ \varepsilon_c\tilde{N}\varepsilon_{cu}\end{cases} \tag{10}$$

where α_1 is the coefficient and always taken as 1.0 if the concrete grade is lower than C50.

The stress and strain of the bolt and plug-in joint should meet the following relations:

$$\begin{cases}\sigma_{st}\tilde{N}f_y\\ \varepsilon_{st}\tilde{N}\varepsilon_u\end{cases},\begin{cases}\sigma_{sj}\tilde{N}f_{yj}\\ \varepsilon_{sj}\tilde{N}\varepsilon_{uj}\end{cases} \tag{11}$$

4.2.2 Joint's load capacity for different failure modes

The strain distribution at the joint after deformation is depicted in Fig. 6. The strain distribution in the compressive zone approximately follows a triangular pattern. Given that the combined splicing joint is assembled by splicing two segments together, the concrete in the tension zone experiences a state of separation, resulting in zero strain. Therefore, only the bolts and plug-in joints exhibit strain in this region. For the sake of representation, the concrete strain is included in Fig. 6, albeit with an actual value of 0.

According to the assumption of the beam plane deformation and the strain triangle similarity relationship, the relationship between the bolt tensile strain and the concrete compressive strain is described as:

$$\frac{\varepsilon_c}{\varepsilon_{st}}=\frac{x_c}{h_0-x_c}=\frac{x}{\beta_1 h_0-x} \tag{12}$$

where h_0 is the effective height of the concrete section, i.e., the distance between the joint force point of the longitudinal tension bolt and the compression sectional edge, $h_0=h-a_s$; h is the segment thickness; a_s is the distance between the bolt joint force point and the tension edge of the concrete section; and x_c is the height of the neutral axis controlled by the plane section assumption, $x_c=x/\beta_1$. β_1 is the coefficient and taken as 0.8 if the concrete grade is lower than C50.

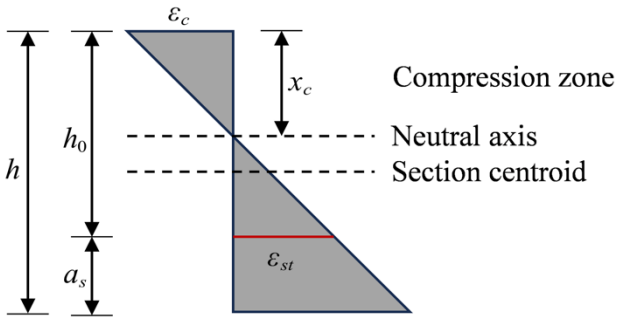

Fig. 6. Strain distribution at the joint of the combined splicing joint

Since the stress-strain response of the concrete, bolts, and plug-in joints is simplified as elastic-ideal plasticity, it is necessary to determine whether the concrete, bolts, or plug-in joints reach the ultimate state first before the ultimate load capacity of the combined splicing joint can be calculated.

Bolts and plug-in joints reach the ultimate state first: When the bolts and plug-in joints first reach the ultimate state, $\sigma_{st} = f_y$, $\sigma_{sj} = f_{yj}$, and $\varepsilon_{st} = \varepsilon_{sj} = \varepsilon_u$. Then, Eq. (12) can be rewritten as:

$$\varepsilon_c = \frac{\varepsilon_u x}{\beta_1 h_0 - x} \tag{13}$$

By substituting Eq. (13) into Eq. (5), the stress of the concrete can be obtained as:

$$\sigma_c = E_{ce} \frac{\varepsilon_u x}{\beta_1 h_0 - x} \tag{14}$$

Substituting Eq. (14) into Eq. (9) yields the following:

$$N + f_y n_1 A_s + f_{yj} n_2 A_{sj} = E_{ce} \frac{\varepsilon_u x}{\beta_1 h_0 - x} bx \tag{15}$$

The height of the concrete compressive zone x can be calculated by Eq. (15); then, it can be substituted back into Eqs. (13) and (14). The concrete compressive strain and stress can be calculated, and the stress state of the concrete can be determined by Eq. (16):

$$\begin{cases} \sigma_c \tilde{\mathrm{N}} \alpha_1 f_c \\ \varepsilon_c \tilde{\mathrm{N}} \varepsilon_0 \end{cases} \tag{16}$$

If the concrete compressive strain ε_c and stress σ_c can meet Eq. (16), then the concrete has not yet reached the yield state, but the bolts and plug-in joints have yielded firstly. If Eq. (16) is not satisfied, then the concrete has reached the yield state before the bolts and plug-in joints reach the ultimate state, and the ultimate bending moment of the combined splicing joint cannot be determined by the method mentioned above.

When the above conditions are met, the bolts and plug-in joints yielded, and the concrete is still in the elastic state. The ultimate moment of the combined splicing joint is determined according to the balance condition of the torque in Fig. 5.

Taking the moment of the concrete centre in the compressive zone yields the following:

$$M_u = \left(f_y n_1 A_s + f_{yj} n_2 A_{sj} \right) \left(h_0 - \frac{x}{2} \right) + N \left(\frac{h}{2} - \frac{x}{2} \right) \tag{17}$$

Taking the moment of the resultant point of the bolts and plug-in joints can yield:

$$M_u = E_{ce} \varepsilon_c bx \left(h_0 - \frac{x}{2} \right) - N \left(\frac{h}{2} - \frac{x}{2} \right) \tag{18}$$

Concrete reaches the ultimate state first: If the concrete yields firstly, with $\sigma_c = \alpha_1 f_c$ and $\varepsilon_c = \varepsilon_{cu}$, Eq. (13) can be rewritten as follows:

$$\varepsilon_{st} = \varepsilon_{cu} \frac{\beta_1 h_0 - x}{x} \tag{19}$$

By substituting Eq. (19) into Eq. (11), the stress of the bolts can be obtained:

$$\sigma_{st} = E_s \varepsilon_{cu} \frac{\beta_1 h_0 - x}{x} \tag{20}$$

By substituting Eq. (19) into Eq. (12), the stress of the plug-in joints can be obtained as:

$$\sigma_{sj} = E_{sj} \varepsilon_{cu} \frac{\beta_1 h_0 - x}{x} \tag{21}$$

Substituting Eqs. (20) and (21) into Eq. (22) yields the following:

$$N + E_s \varepsilon_{cu} \frac{\beta_1 h_0 - x}{x} n_1 A_s + E_{sj} \varepsilon_{cu} \frac{\beta_1 h_0 - x}{x} n_2 A_{sj} = \alpha_1 f_c bx \tag{21}$$

The concrete compressive zone height can be calculated according to Eq. (22) and then substituted back into Eqs. (19), (20) and (21). The tensile strain and stress of the bolts and plug-in joints can be calculated, and the stress state of the bolts and plug-in joints can be determined via Eq. (23):

$$\begin{cases} \sigma_{st} \tilde{\mathrm{N}} f_y \\ \varepsilon_{st} \tilde{\mathrm{N}} \varepsilon_y \end{cases}, \quad \begin{cases} \sigma_{sj} \tilde{\mathrm{N}} f_{yj} \\ \varepsilon_{sj} \tilde{\mathrm{N}} \varepsilon_y \end{cases} \tag{23}$$

If the tensile strain ε_{st} and tensile stress σ_{st}, σ_{sj} of the bolts and plug-in joints can meet Eq. (23), then the bolts and plug-in joints have not yet yielded, but the concrete has yielded. If Eq. (23) is not satisfied, then the bolts and plug-in joints have reached the yield state before the concrete reaches the ultimate state.

When the above conditions are met, the concrete first yields, and the bolts and plug-in joints are still in the elastic state. The joint's ultimate moment is determined according to the balance conditions of the torque in Fig. 6.

Taking the moment of the concrete centre in the compressive zone yields:

$$M_u = \left(E_s \varepsilon_{st} n_1 A_s + E_{sj} \varepsilon_{st} n_2 A_{sj} \right) \left(h_0 - \frac{x}{2} \right) + N \left(\frac{h}{2} - \frac{x}{2} \right) \tag{24}$$

Taking the moment of the resultant point of the bolts and plug-in joints can yield:

$$M_u = \alpha_1 f_c bx \left(h_0 - \frac{x}{2} \right) - N \left(\frac{h}{2} - a_s \right) \tag{25}$$

Concrete, bolts, and plug-in joints all reach the yield state: At this time, the height of the compressive zone x calculated according to the elasticity in the above two cases is no longer applicable, and it is necessary to recalculate the height of the compressive zone x according to Eq. (26):

$$N + f_y n_1 A_s + f_{yj} n_2 A_{sj} = \alpha_1 f_c b x \tag{26}$$

The height of the concrete compressive zone x is subsequently substituted into Eqs. (26) or (25) to calculate the ultimate bending moment of the combined splicing joint.

4.2.3 Calculation results of the load capacity

These equations above are applied to calculate the ultimate bending moments of specimens JT0, JT1, JT2 and JT3 mentioned above. For these specimens the bolts and plug-in joints, first reach the ultimate state. Then, the values of the parameters required for calculating the ultimate bending moment are $f_y = 400\text{MPa}$, $f_{yj} = 335\text{MPa}$, $A_s = 113\text{mm}^2$, $A_{sj} = 64\text{mm}^2$, $E_{ce} = 11.6\text{GPa}$, $\varepsilon_u = 0.01$, $\beta_1 = 0.8$, $h_0 = 87\text{mm}$, and $b = 600\text{mm}$.

The calculation results from the equations established in this section are the ultimate bending moment of the combined splicing joint, whereas the measured data are the vertical load of the combined splicing joint. Therefore, the vertical load should be converted into the bending moment through force analysis. The left half of the combined splicing joint is taken as the research object. A diagram of the force in the loading process is illustrated in Fig. 7.

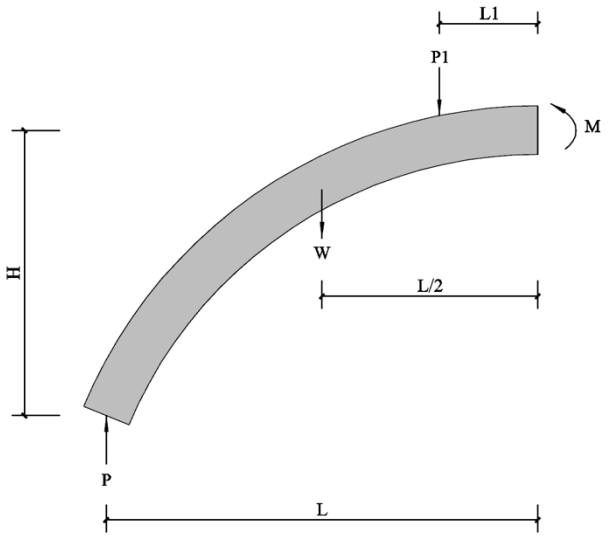

Fig. 7. Force of the combined splicing joint left half

Taking the moment of the combined splicing joint left support, the bending moment at the joint of the combined splicing joint can be calculated, as shown in Eq. (27):

$$M = P1\left(L - L1\right) + \frac{WL}{2} \tag{27}$$

where $P1$ is half of the vertical load at the joint of the combined splicing joint; W is the gravity of the combined splicing joint; L is the horizontal distance between the joint and support of the combined splicing joint; and $L1$ is the horizontal distance between the joint and the vertical load of the combined splicing joint.

The calculated bending moments of each specimen are summarized in Table 2. To further verify the suggested method, the calculated results and test ones are compared in Table 2.

Table 2. Comparison of the calculated and tested load capacities of the combined splicing joint

Specimen number	Calculated value (kN·m)	Test value (kN·m)	Relative error (%)
JT0	10	10.7	7.0
JT1	11.7	13.2	12.8
JT2	13.4	15.3	14.2
JT3	15.1	18.3	21.2

5. Conclusions

A new type of combined splicing joint for tunnel segments in complex geological conditions was proposed, and its mechanical performances were investigated. The main conclusions were obtained as following :

(1) The addition of a plug-in joint to the traditional segmental joint enhances the joint's bending stiffness. Compared to specimen JT0, the bending stiffness of specimen JT1 is increased by 50%. By incorporating a plug-in joint, the load capacity of the segmental joint can be improved to a certain extent, with the degree of increase reaching 25%.

(2) For the combined splicing joint, the incorporation of a plug-in joint improves its load capacity. As the number of plug-in joints increases, the improvement in load capacity becomes more pronounced. Additionally, the load capacity of the segmental joint can be further enhanced by adjusting the position of the plug-in joints.

(3) The combined splicing joint is simplified into a beam model, with the bolts treated as steel bars. A load capacity calculation formula is derived using the calculation method for concrete structures. When the final calculation results are compared with experimental data, the results indicate that the load capacity calculation formula designed in this paper is reasonable.

This study primarily focuses on the mechanical performances of the combined splicing joints. It is important to note that the test specimens used are smaller than those typically employed in practice. As a next step, full-scale experimental investigations should be conducted to validate the findings of this study.

Acknowledgements

The work was supported by Fujian Province Guiding Project (2021Y0026).

This is an Open Access article distributed under the terms of the Creative Commons Attribution License.

References

[1] N. A. Do, D. Dias, P. Oreste, and I. Djeran-Maigre, "2D numerical investigation of segmental tunnel lining under seismic loading," *Soil Dyn. Earthq. Eng.*, vol. 72, pp. 66-76, May 2015. doi:10.1016/j.soildyn.2015.01.015.

[2] X. L. Gan, X. N. Gong, N. W. Liu, J. L. Yu, and W. B. Li, "Random analysis method for nonlinear interaction between shield tunnel and spatially variable soil," *Comput. Geotech.*, vol. 166, Dec. 2023, Art. no. 105964. doi: 10.1016/J.COMPGEO.2023.105964.

[3] Ruiz López, A. Tsiampousi, J. R. Standing, and D. M. Potts, "A new model for simulating the behaviour of grey cast iron tunnel joints with structural elements in geotechnical analysis," *Eng. Struct.*, vol. 304, Apr. 2024, Art. no. 105964. doi:10.1016/j.engstruct.2023.117354.

[4] C. J. Gong, W. Q. Ding, K. M. Mosalam, S. Günay, and K. Soga, "Comparison of the structural behavior of reinforced concrete and steel fiber reinforced concrete tunnel segmental joints," *Tunn. Undergr. Sp. Tech.*, vol. 68, pp. 38-57, Sep. 2017. doi: 10.1016/j.tust.2017.05.010.

[5] Sharghi, H. Afshin, D. Dias, and H. Jeong, "3D numerical study of the joint dislocation and spacing impacts on the damage of tunnel segmental linings," *Structures*, vol. 56, Oct. 2023, Art. no. 104878. doi:10.1016/j.istruc.2023.104878.

[6] N. A. Do, D. Dias, P. Oreste, and I. Djeran-Maigre, "A new numerical approach to the hyperstatic reaction method for segmental tunnel linings," *Int. J. Numer. Anal. Met.*, vol. 38, no. 15, pp. 1617-1632, Oct. 2014. doi: 10.1002/nag.2277.

[7] M. Nematollahi, H. Molladavoodi, and D. Dias, "Three-dimensional numerical simulation of the Shiraz subway second line-influence of the segmental joints geometry and of the lagging distance between twin tunnels' faces," *Eur. J. Environ. Civ. En.*, vol. 24, no. 10, pp. 1606-1622, Aug. 2020. doi: 10.1080/19648189.2018.1476270.

[8] A. R. López, A. Tsiampousi, J. R. Standing, D. M. Potts, "A new model for simulating the behaviour of grey cast iron tunnel joints with structural elements in geotechnical analysis, " *Eng. Struct.*, vol. 304, Apr. 2024, Art. no. 117354. doi: 10.1016/j.engstruct.2023.117354.

[9] X. Liu, Y. Bai, Y. Yuan, and H. A. Mang, "Experimental investigation of the ultimate bearing capacity of continuously jointed segmental tunnel linings," *Struct. Infrastruct. Eng.*, vol. 12, no. 10, pp. 1364-1379, Oct. 2016. doi: 10.1080/15732479.2015.1117115.

[10] A. Rashiddel, M. Hajihassani, M. Kharghani, H. Valizadeh, R. Rahmannejad, and D. Dias, "Numerical analysis of segmental tunnel linings-Use of the beam- spring and solid-interface methods," *Geomech. Eng.*, vol. 29, no. 4, pp. 471-486, May 2022. doi:10.12989/gae.2022.29.4.471.

[11] L. Zhang, K. Feng, M. R. Li, C. He, M. Q. Xiao, and Z. Zhang, "Characteristic analysis on the compression-bending capacity of segmental joint based on the investigated joint parameters," *Tunn. Undergr. Sp. Tech.*, vol. 102, 2020, Art. no. 103444. doi: 10.1016/j.tust.2020.103444.

[12] M. J. Avanaki, M. Abedi, and A. Hoseini, "Experimental and numerical-based design of hybrid steel fibre-reinforced concrete tunnels," *Mag. Concrete Res.*, vol. 72, no. 14, pp. 720-733, Jul. 2020. doi:10.1680/jmacr.18.00279.

[13] W. Q. Guo, K. Feng, Y. L. Zhou, W. Q. Yang, X. Y. Lu, M. Q. Xiao and C. He, "Full-scale test and numerical modeling on deformation and damage behavior of segmental joints under ultimate compression-bending load," *Eng. Struct.*, vol. 279, 2023, Art. no. 115648. doi: 10.1016/J.ENGSTRUCT.2023.115648.

[14] L. Zhang, K. Feng, P. K. Xu, C. He, and H. H. Zhang, "Refined three-dimensional numerical model for segmental joint and its application," *Struct. Concr.*, vol. 21, no. 4, pp. 1612-1624, Apr. 2020. doi: 10.1002/suco.201900550.

[15] J. Oh and T. Moon, "Seismic design of a single bored tunnel: longitudinal deformations and seismic joints," *Rock Mech. Rock Eng.*, vol. 51, no. 3, pp. 893-910, Mar. 2018. doi:10.1007/s00603-017-1366-0.

[16] B. A. Boye, S. J. Abbey, S. Ngambi, and J. Fonte ,"Development of improved models for estimation of bursting stresses in elements under high-concentrated load," *Lat. Am. J. Soilds Stru.*, vol. 16, no. 1, Jan. 2019, Art. no. e156. doi: 10.1590/1679-78255031.

[17] N. Allahverdi, M. Bakhshi, M. Partovi, and V. Nasri, "3D-nonlinear finite element analysis of staged shield-driven tunnel excavation with a focus on response of segmental tunnel linin," *Geomech. Tunnel.*, vol. 16, no. 1, pp. 60-67, Feb. 2023. doi:10.1002/geot.202200071.

[18] K. Yang, Q. X. Yan, and C. Zhang, "Three-dimensional mesoscale numerical study on the mechanical behaviors of SFRC tunnel lining segments," *Tunn. Undergr. Sp. Tech.*, vol. 113, 2021, Art. no. 103982. doi: 10.1016/J.TUST.2021.103982.

[19] H. B. Xu, Q. C. Liu, B. T. Li and C. R. Guo, "Identification of shield tunnel segment joint opening based on annular seam pressure monitoring," *Sensors*, vol. 24, no. 12, Jun. 2024, Art. no. 3924. doi: 10.3390/S24123924.

[20] T. Cordes, K. Mair am Tinkhof, R. Crapp, and N. Radončić, "Geomechanical loading of the segmental linings of the Brenner Base Tunnel," *Geomech. Tunnel.*, vol. 17, no. 1, pp. 52-63, Feb. 2024. doi:10.1002/geot.202300053.

[21] S. R. Wang, X. G. Wu, J. H. Yang, J. Q. Zhao, and F. L. Kong, "Mechanical behavior of lightweight concrete structures subjected to 3D coupled static-dynamic loads," *Acta Mech.*, vol. 231, no. 11, pp. 4497-4511, Nov. 2020. doi:10.1007/s00707-020-02739-y.

[22] P. Xu, Y. H. Cui, J. F. Dai, S. R. Wang, M. X. Zhang, and Z. G. Hou, "Mechanical performance of texttile reinforced concrete containing steel fibers and basalt fibers dubjected to high temperatures," *Ceram-Silikáty*, vol. 65, no. 3, pp. 263-272, Jul. 2021. doi: 10.13168/cs.2021.0027.

[23] N. Gottardi, S. Freitag, and G. Meschke, "Real-time estimation of the structural utilization level of segmental tunnel lining," *Undergr. Space*, vol. 17, pp. 132-145, Aug. 2024. doi:10.1016/j.undsp.2023.11.011.

[24] X. G. Wu, S. R. Wang, J. H. Yang, J. Q. Zhao, and X. Chang, "Damage characteristics and constitutive model of lightweight shale ceramsite concrete under static-dynamic loading," *Eng. Fract. Mech.*, vol. 259, Jan. 2022, Art. no. 108137. doi:10.1016/j.engfracmech.2021.108137.

[25] F. Rauch and O. Fischer, "Application of a structural monitoring on segmental tunnel linings," *Struct. Concrete*, vol. 24, no. 6, pp. 7779-7793, Dec. 2023. doi:10.1002/suco.202300141.

[26] Y. L. Lin, X. W. Wang, J. Gong, S. R. Wang, H. S. Sun, and H. H. Liu, "Seismic performance of an exterior joint between a square steel tube column and an H-shape steel beam," *Sustainability*, vol. 15, no. 4, Feb. 2023, Art. no. 3856. doi:10.3390/su15043856.

[27] F. Rauch and O. Fischer, "Structural behavior of segmental tunnel linings based on in situ measurements," *J. Perform. Constr. Fac.*, vol. 38, no. 4, Aug. 2024, Art. no. 4688. doi:10.1061/JPCFEV.CFENG-4688.J PERFORM CONSTR FAC.

[28] A. Rashiddel, M. Kharghani, D. Daniel, and M. Hajihassani, "Numerical study of the segmental tunnel lining behavior under a surface explosion-Impact of the longitudinal joints shape," *Comput. Geotech.*, vol. 128, Dec. 2020, Art. no. 103822. doi:10.1016/j.compgeo.2020.103822.

[29] M. Nematollahi, H. Molladavoodi, and D. Dias, "Three-dimensional numerical simulation of the Shiraz subway second line-influence of the segmental joints geometry and of the lagging distance between twin tunnels' faces," *Eur. J. Environ. Civ. En.*, vol. 24, no. 10, pp. 1606-1622, Aug. 2020. doi:10.1080/19648189.2018.1476270.

[30] J. Gollegger, "Experience from pre-excavation and leakage closing injections obtained in the Follo Line Project," *Geomech. Tunnel.*, vol. 15, no. 5, pp. 550-554, Oct. 2022. doi: 10.1002/geot.202200010.